Heteroepitaxial diamond films on silicon (001): Interface structure and crystallographic relations between film and substrate

C. L. Jia and K. Urban
Institut für Festkörperforschung, Forschungszentrum Jülich GmbH, D-52425 Jülich, Germany

X. Jiang
Fraunhofer-Institut für Schicht- und Oberflächentechnik, D-38108 Braunschweig, Germany
(Received 13 March 1995)

The interfaces between highly (001)-oriented diamond films and the silicon (001) substrates were investigated by high-resolution electron microscopy. It was found that heteroepitaxially oriented grains which exhibit a defined orientation relationship to the substrate lattice grow directly on the clean silicon surface. The majority of the grains observed have their basic axes parallel or almost (within a few degrees) parallel to the basic axes of silicon. In addition, grains with about 14° and 70° rotation around a ⟨110⟩ axis are also observed. In the latter case the lattice is in twin relation to that of the ideally oriented nonrotated grains. In all cases the interface structure is well defined and the angular deviation of the two lattices is compensated by appropriate interface dislocations. These dislocations are either of the 60° type or are Lomer dislocations formed by the reaction of two types of 60° dislocations. The observed orientation relationships can be explained on the basis of the near-coincidence-site lattice of the two materials.

I. INTRODUCTION

While diamond films have been synthesized routinely for more than a decade, it has only recently become possible to grow continuous diamond films on silicon substrates with the majority of the grains in heteroepitaxial orientation.[1,2] This important step toward technical application has stimulated further work concerning details of the deposition processes and the structural properties of these films which are grown on (001)-oriented substrates. The morphology can be studied by scanning electron microscopy as soon as the film thickness has reached a few micrometers. It was found that the films consist of flat square-shaped (001)-oriented grains with their edges parallel to crystallographic ⟨110⟩ directions.[1] There is usually a small misorientation angle of a few degrees among these grains and between some of the diamond grains and the silicon substrate. The thermodynamics and kinetics of diamond nucleation on silicon have been investigated by Jiang, Schiffmann, and Klages.[3] Several sites for diamond nucleation were reported, i.e., on an amorphous layer, on a β-SiC layer, or directly on the clean Si surface.[4–6] It was found that the morphology of grains grown on amorphous layers is different from that of grains which grow on the clean Si surface.[7] In the former case a nanocrystalline structure with random orientations was observed, while, in the latter case, the grains had a relatively large diameter of 0.1 μm or more and exhibited special orientation relations with respect to the silicon substrate.

Although it has been demonstrated[8,9] that deposition parameters play an important part in the growth competition of differently oriented grains, it is obviously desirable to form the diamond nuclei of the proper orientation at a very early stage of growth. In order to better understand the conditions which govern nucleation and growth it is not only necessary to study the interfaces and the structural details of the deposition products, but also to investigate the basic crystallographic relations between the two materials. In the present work the interface between highly (001)-oriented diamond films and the silicon substrate was studied in cross section by high-resolution transmission electron microscopy. In consideration of the small lattice parameter of diamond and the resolution limit of the microscope, the viewing direction was chosen along the crystallographic [1$\bar{1}$0] direction of the silicon substrate. Our emphasis is on a structural characterization of the [1$\bar{1}$0] tilt interfaces which, under these conditions, are imaged edge on.

II. EXPERIMENT

The diamond films were prepared by microwave-plasma-assisted chemical vapor deposition in an ASTEX 1.5-kW reactor on mirror-polished (001)-oriented silicon substrates. The experimental details have been published.[10] Prior to insertion into the deposition chamber the substrates were ultrasonically cleaned in acetone. None of the conventional *ex situ* techniques for enhancement of diamond nucleation, such as scratching or coating with amorphous carbon, were used. During the deposition of the films, the substrate temperature was kept at about 800 °C.

The films had a thickness of less than 1 μm. Cross-section specimens for electron microscopy were prepared by cutting the diamond-silicon chips into slices in such a way that the normal of the final specimen was parallel to the [1$\bar{1}$0] direction of the silicon substrate. Then two of these slices were glued together face to face. After mechanically grinding and dimpling, these specimens

0163-1829/95/52(7)/5164(8)/$06.00

were ion milled to perforation. High-resolution electron microscopy was performed in a JEOL 4000EX electron microscope operated at 400 keV.

III. ELECTRON-MICROSCOPIC RESULTS

Figure 1 shows a low-magnification overview of the diamond film recorded with the electron beam parallel to the $[1\bar{1}0]$ zone axis of the substrate. The film is obviously polycrystalline. Nevertheless, the majority of the grains exhibit a good orientation, i.e., their (001) axes are parallel to the (001) axis of the substrate or make only a small angle with it. In projection, the grains are of polygonal shape with their edges parallel to low-index planes. The edge marked by small white arrows is the projection of the (001) plane.

Twins are frequently observed in the diamond grains. They start from the interface between the film and substrate. Smaller grains occasionally occur between well-oriented grains exhibiting a random orientation with respect to the substrate. There is usually an amorphous layer between these randomly oriented grains and the silicon substrate, as previously reported by Tzou *et al.*[7]

On a larger scale, the interface is flat and parallel to the (001) plane of the substrate, as shown in Fig. 1. On a nanometer scale, however, it exhibits quite a rough morphology. Figure 2 displays a lattice fringe picture of an interface where the diamond crystal grows in ideal orientation, i.e., epitaxially with its basic axes parallel to those of the silicon substrate. The arrows indicate the orientation of both the diamond and silicon lattices. The roughness of the interface structure gives rise to contrast inhomogeneities along the boundary. In particular, some areas near the interface show a modulationlike contrast.

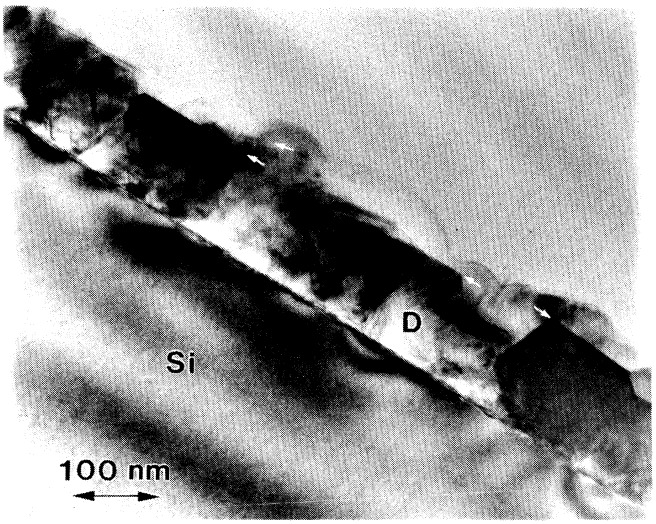

FIG. 1. A low-magnification overview of a highly (001)-oriented diamond film (D) on a (001) silicon substrate (Si). The viewing direction is parallel to the $[1\bar{1}0]$ zone axis of silicon. The well-oriented grains of diamond exhibit a polygonal morphology. Small arrows indicate the projected (001) plane of the diamond grains.

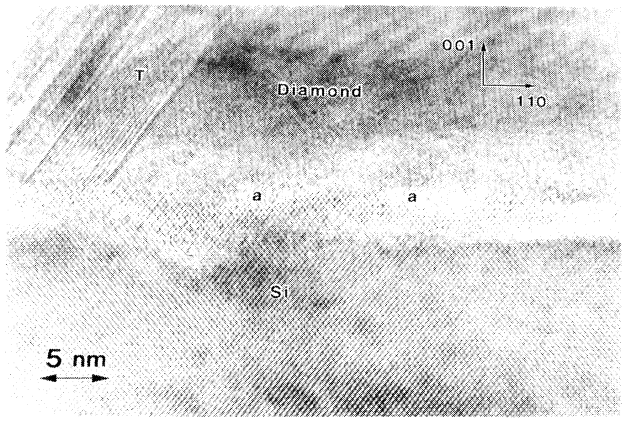

FIG. 2. A $[1\bar{1}0]$ lattice-fringe picture of the interface between a diamond grain and the silicon substrate. The diamond grain is oriented with its basic axes parallel to those of the silicon substrate (ideal orientation). Two small amorphous zones in the interface are marked by *a*. Twin lamellae (*T*) are visible on the left-hand side of the diamond grain.

This results from the overlap of the two materials along the viewing direction, since the roughness also exists in this direction. Nevertheless, the continuity of the lattice fringes across the interface of the substrate and the diamond crystal is obvious. Two small amorphous areas are visible which are denoted by *a*. As reported previously,[7] these areas may be related to silicon oxide remnants not removed during the polishing process. In the area on the upper left we see twin lamellae which start from the interface. One of the twins (marked by *T*) exhibits a lattice-fringe periodicity three times as large as the basic fringe pattern along the $[11\bar{1}]$ direction. This periodicity can be explained by the overlap of two twin lamellae along the viewing direction.[11]

Figure 3 presents a lattice-fringe picture of an interface

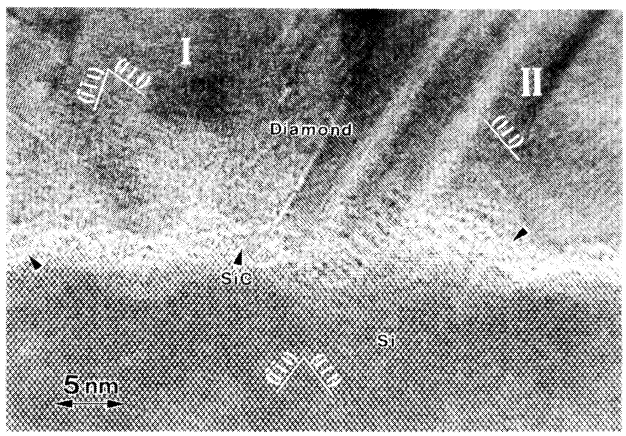

FIG. 3. Interface of two diamond grains to the silicon substrate. The two grains deviate from the ideal orientation by a rotation around the $[1\bar{1}0]$ axis (grain I) and the [111] axis (grain II). Small β-SiC particles are denoted by arrowheads. The basic axes of these precipitates are parallel to those of silicon.

region where two diamond grains with different lattice orientations, grains I and II, join. For grain I the electron beam is still parallel to the $[1\bar{1}0]$ zone axis. However, the grain is rotated around this axis and therefore is misaligned with respect to the substrate. This becomes obvious if one follows the fringes of the $(\bar{1}\,\bar{1}1)$ planes of silicon across the interface where the corresponding $(\bar{1}\,\bar{1}1)$ planes of diamond make an angle with the Si fringes. In grain II only a single set of (111) lattice fringes can be seen, which indicates a deviation of the orientation of its $[1\bar{1}0]$ zone axis caused by a rotation around an axis which is perpendicular to the (111) plane. In this case, the (111) planes of the grain II are well imaged and almost parallel to those of silicon.

The area of Fig. 3 also contains small β-SiC grains a few manometers in diameter (marked by arrowheads). Their structure was identified on the basis of optical diffractograms obtained by focusing a laser beam on the small grain area in the electron-microscopic negative. The β-SiC grains exhibit a defined orientation relationship with respect to the substrate, i.e., the basic axes are parallel to those of silicon. This orientation relationship is independent of the orientation of the adjoining diamond grains.

Figure 4 shows a high-magnification lattice-fringe picture of the interface between an ideally oriented diamond grain and the substrate. No secondary phases occur in the interface area. The small open circles mark the connection of the $\{111\}$ planes of the two materials at the interface. Regarding the image at a glancing angle along the two sets of $\{111\}$ planes, it becomes obvious that the large lattice mismatch between silicon (lattice parameter $a_{Si}=0.543$ nm; subscripts Si for silicon and D for diamond are used throughout this paper) and diamond ($a_D=0.357$ nm) is accommodated by the introduction of a 3:2 registry (with 1.5% mismatch) for the diamond lattice with respect to that of silicon. Following the lattice from the substrate, across the interface, to the diamond crystal we find that every third lattice plane of diamond terminates at the interface. Each $\{111\}$-terminating plane corresponds to a misfit dislocation which has the character of a 60° dislocation with a Burgers vector of $\frac{a}{2}\langle 110\rangle$.

Each type of terminating plane has two possible Burgers vectors which can be identified in the $[1\bar{1}0]$ lattice image. The dislocations related to the (111)-terminating planes possess a Burgers vector of either $\frac{a}{2}[101]$ or $\frac{a}{2}[011]$. The two Burgers vectors have the same projected component, $\frac{a}{4}[112]$, along the $[1\bar{1}0]$ viewing direction, as is demonstrated by a Burgers circuit composed of the small arrows in Fig. 4. The two possible Burgers vectors for the dislocations related to the $(\bar{1}\,\bar{1}1)$-terminating planes are either $\frac{a}{2}[01\bar{1}]$ or $\frac{a}{2}[10\bar{1}]$, which have a projected value of $\frac{a}{4}[\bar{1}\,\bar{1}2]$. Since there is no misorientation between this diamond grain and the silicon substrate, the two types of $\{111\}$-terminating planes occur in equal numbers. This is demonstrated by the computer-created Fourier-filtered images displayed in Fig. 5. These images were synthesized by using only one row of $\{111\}$-type spots of the power spectrum (shown as an inset) of the image shown in Fig. 4. The upper fringe pattern was, as indicated by the thick arrows in the inset, formed by the row of (111)-type spots and the lower

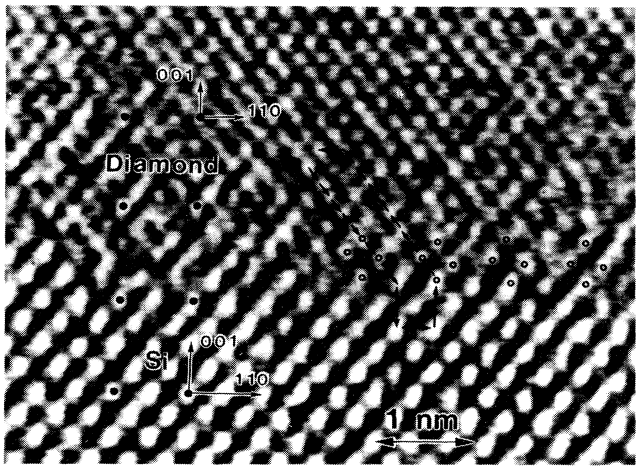

FIG. 4. A $[1\bar{1}0]$ lattice-fringe image of the interface between diamond and silicon. The diamond grain has a perfectly epitaxial orientation. The small circles allow the continuity of the two lattices across the interface to be verified. A Burgers circuit composed of small arrows demonstrates the Burgers vector of the dislocations which are related to the terminating $\{111\}$-type planes at the interface. The black dots indicate a $\Sigma_D 54/\Sigma_{Si}$ 16 near-coincidence-site lattice (NCSL).

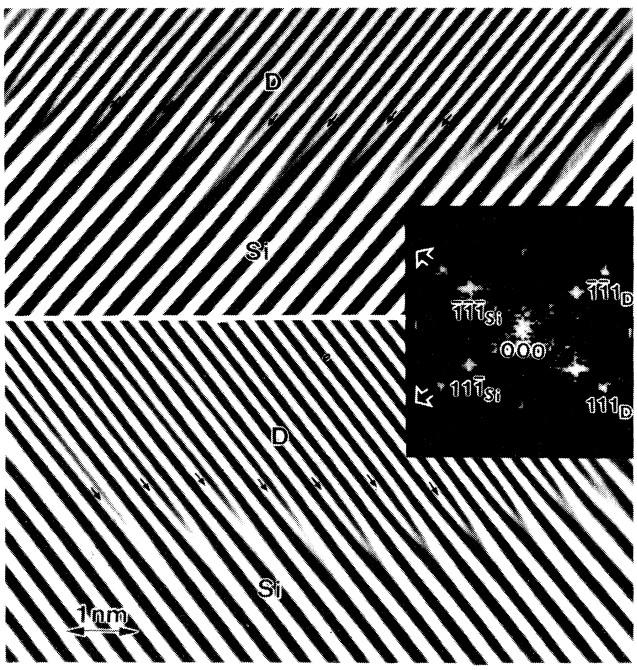

FIG. 5. Lattice-fringe pattern obtained by Fourier filtering the image of the Fig. 4. In the image synthesis the (111)-spot row (upper picture) and the $(\bar{1}\,\bar{1}1)$-spot row (lower picture) of the corresponding power spectrum were used, which is shown as an inset. Small arrows mark the terminating planes at the interface.

fringe pattern by the $(\bar{1}\,\bar{1}1)$-type spots.

In Fig. 4 the contrast close to the interface is irregular, and the exact position of the interface plane is difficult to identify, although it can be localized within 2–3 atomic layers. A possible explanation for this is the high density of misfit dislocations whose local strain fields introduce irregularities into the image contrast. Another reason is that the orientation of the interface plane deviates by a small angle from the exact (001) orientation and therefore is inclined along the viewing direction. A periodicity which is common for both silicon and diamond can be identified in the figure. It is denoted by black dots. It is the periodicity of the near-coincidence-site lattice (NCSL) which characterizes the interface, and which will be discussed in Sec. IV.

In many cases, the orientation of the diamond grains deviates slightly, i.e., by a few degrees, from the ideal one. Nevertheless, these grains also nucleate directly on the substrate and exhibit a well-defined structural relation to the substrate lattice. In this case, the sum of the Burgers vectors of the two sets of misfit dislocations yields a component perpendicular to the interface plane. Figure 6 shows an example. The diamond grain in this image has a deviation of 4° from the ideal orientation by a rotation around the common (silicon and diamond) $[1\bar{1}0]$ zone axis. This small deviation is compensated for by varying the number of the two types of $\{111\}$ planes which are parallel to the $[1\bar{1}0]$ direction and which terminate at the interface. This can be seen in the figure when the picture is regarded at a glancing angle along the $(\bar{1}\,\bar{1}1)$ and (111) fringes. Figure 7 shows the Fourier-filtered image. about $\frac{2}{7}$ of the (111) planes terminate at the interface in the upper picture of the figure, while a termination of about $\frac{2}{5}$ of the $(\bar{1}\,\bar{1}1)$ planes is visible in the lower picture. The variation of the numbers of the individual terminating planes occurs in such a way that their total number is almost unchanged with respect to the case of the ideal orientation. The component of the sum of the Burgers vectors perpendicular to the interface plane, which is required for accommodation of the small angle misorientation, directly corresponds to the difference in the number of the two types of terminating planes.

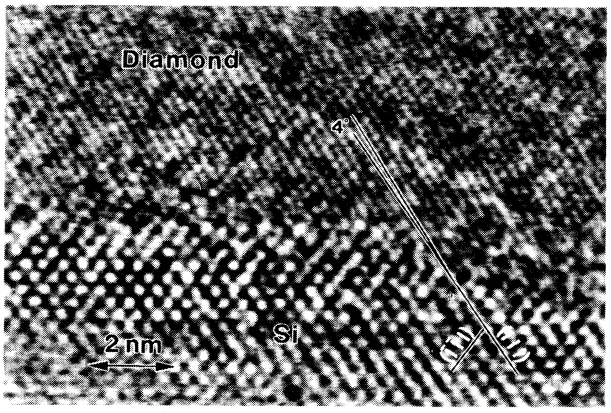

FIG. 6. A $[1\bar{1}0]$ lattice-fringe image showing a diamond grain which exhibits a 4° deviation from the ideal orientation. Such small-angle deviations are compensated for by unequal numbers of the $(\bar{1}\,\bar{1}1)$ and (111) terminating planes.

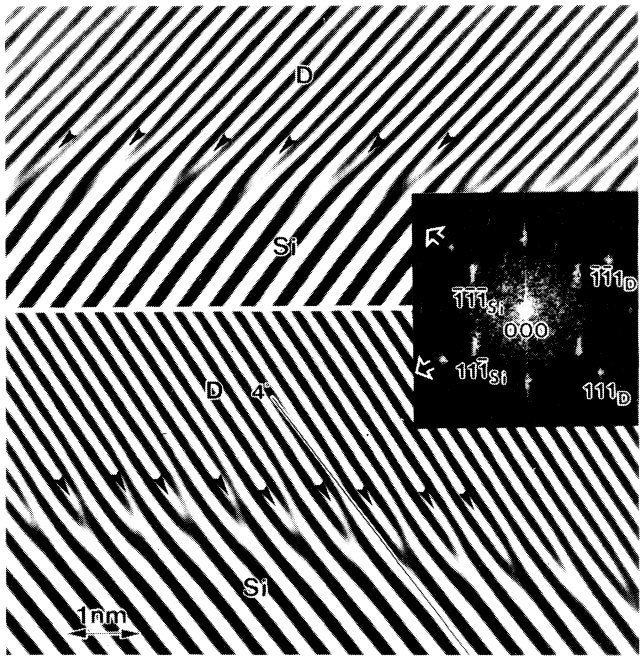

FIG. 7. Fourier-filtered images obtained from Fig. 6 by using the (111)-spot row (upper picture) and the $(\bar{1}\,\bar{1}1)$-spot row (lower picture) of the corresponding power spectrum shown as an inset. They show a different configuration of the terminating planes (marked by arrowheads) in comparison with the ideal situation (Fig. 5).

In the diamond film, we also observed grains with a large angle ($>10°$) misorientation whose lattice nevertheless exhibits a defined orientation relationship to the substrate lattice. A particular type of misorientation observed is based on a tilt angle of about 70° around the common $[1\bar{1}0]$ axis. In this case, one set of the $\{111\}$ planes of diamond (D) is parallel to one type of $\{111\}$ planes in the substrate. At the interface the (111)-type planes of the two materials follow the 3:2 registry. The orientation relationship can be characterized by $(1\bar{1}0)_D \| (1\bar{1}0)_{Si}$, $[221]_D \| [001]_{Si}$, and $[11\bar{4}]_D \| [110]_{Si}$. This kind of diamond grains has a twin relation to those which have the ideal epitaxial orientation.

Figure 8 shows another type of interface. The diamond crystal is tilted around the $[1\bar{1}0]$ direction by 14°. In this case we have an orientation relation of $(1\bar{1}0)_D \| (1\bar{1}0)_{Si}$, $[116]_D \| [001]_{Si}$, and $[33\bar{1}]_D \| [110]_{Si}$. This relation is indicated by the three orthogonal pairs of arrows in the figure. The image clearly demonstrates a direct connection of the lattices of the two materials across the interface. The contrast is harp enough to allow steps with a height of a monatomic layer of silicon to be identified. For this orientation relation, the difference

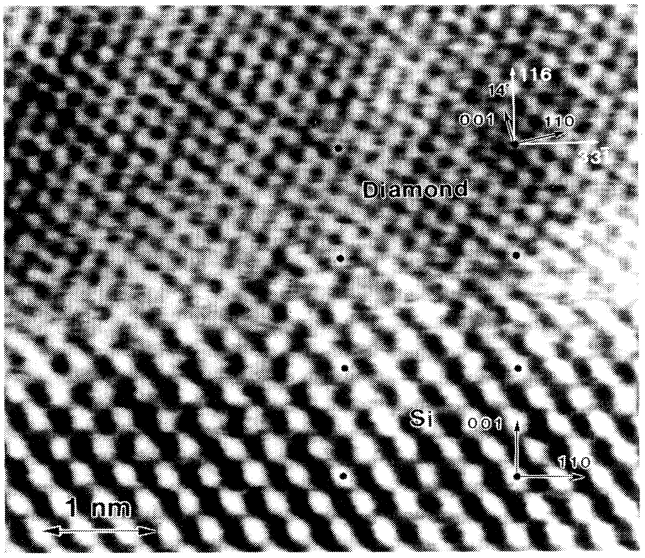

FIG. 8. The interface between a diamond grain and the silicon substrate. This grain is rotated by 14° around the [1$\bar{1}$0] axis with respect to the silicon substrate. For this misorientation angle, a $\Sigma_D 57/\Sigma_{Si} 16$ NCSL is formed. The periodicity of the NCSL is marked by black dots.

in the number of the two types of terminating planes is larger than for the interface of Fig. 6. Nevertheless, the sum of the terminating planes at the interface again remains unchanged with resect to the case of the ideal orientation. As a result, the component of the sum of the Burgers vectors perpendicular to the interface is quite large. The black dots indicate a NCSL which is continuous across the interface.

IV. ATOMIC COINCIDENCE RELATIONS BETWEEN DIAMOND AND SILICON

In the silicon/diamond system, the two components have the same structure, but with respect to diamond we have a lattice-parameter misfit of $\delta=(a_S-a_D)/a_D=52\%$. For a 3:2 registry, i.e., three units of diamond facing two units of silicon, in a (001) interface we obtain a much smaller misfit of $\delta=1.5\%$.

The coincidence-site-lattice model (CSL) has been developed for the characterization of grain boundaries in cubic materials.[12] Boundaries of relatively low energy occur for certain misorientations of the two joining grains which yield a particularly dense CSL. The density is characterized by the inverse of the parameter Σ which is given by the CSL unit-cell volume divided by the volume associated with each crystal lattice point. The near-coincidence-site lattice (NSCL) description developed by Baluffi, Brokman, and King[13] is based on a generalization of the CSL model. It is also applicable to heterointerfaces, i.e., boundaries between phases of different structure, where a small distortion of ideal lattices is required in order to produce a conventional coincidence-sites lattice. In the following we employ the term NCSL to denote both the experimentally observed near-coincidence-site lattice (as in Figs. 4 and 8) and the coincidence-site lattice obtained by suitably straining the real lattices in order to produce an exact match of the nearly coinciding atom positions.

As already discussed,[13] in the characterization of heterointerfaces two particular modifications of the usual simple CSL description are involved which are also used in the following for our discussion of the orientation relationships between Si(001) and heteroepitaxial diamond. First of all, the coincidence-site lattice has a basis, i.e., more than one coincident atom site exists for a particular NCSL unit translation vector. Furthermore the NCSL is characterized by two different coincidence parameters, one for the silicon, Σ_{Si}, and one for the diamond lattice, Σ_D. We note that, in contrast to the case of homoboundary structures, Σ need not be an odd number. The values of Σ are given by

$$\Sigma_D=\frac{\omega_{CSL}}{\omega_D}\ , \tag{1a}$$

$$\Sigma_{Si}=\frac{\omega_{CSL}}{\omega_{Si}}\ , \tag{1b}$$

where ω_{CSL} denotes the volume corresponding to each coincidence atom site in the NCSL unit cell (i.e., NCSL cell volume divided by the number of coincidence sites per NCSL unit cell) and ω_D and ω_{Si} denote the atomic volume of silicon and carbon, respectively. Following Balluffi, Brokman, and King,[13] a necessary (though not sufficient) criterion for the formation of low-energy interfaces is that $\Sigma_D/\Sigma_{Si}\approx R$, where $R=\omega_{Si}/\omega_D=3.53$.

The orientation relations between the silicon substrate and the diamond grains derived experimentally from our

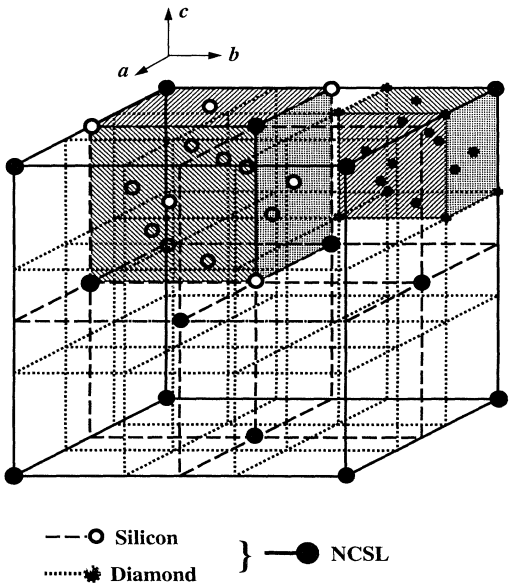

FIG. 9. Perspective view of the $\Sigma_D 54/\Sigma_{Si} 16$ NCSL for the basic axes of diamond parallel to those of silicon. The diamond and silicon unit cells are shaded.

pictures can now be discussed in the framework of the NCSL model. For the ideal heteroepitaxial situation, where the basic axes of the two materials are parallel to each other, we observed a 3:2 registry between diamond and silicon. The unit cell of the corresponding NCSL is shown in Fig. 9. It was obtained by compressingly straining the lattice of silicon by 1.5% (for compensation of the mismatch δ) in order to produce an exact coincidence-site lattice. The basic unit cells of silicon and diamond are shaded. The three-dimensional NCSL is fcc lattice and thus has a basis of 4. The NCSL unit cell comprises eight unit cells of silicon and 27 unit cells of diamond. For the coincidence parameters this yields

$$\Sigma_D = \frac{27\Omega_D}{4} : \frac{\Omega_D}{8} = 54 , \tag{2a}$$

$$\Sigma_{Si} = \frac{8\Omega_{Si}}{4} : \frac{\Omega_{Si}}{8} = 16 , \tag{2b}$$

$$\frac{\Sigma_D}{\Sigma_{Si}} = 3.38 , \tag{2c}$$

where Ω_D and Ω_{Si} denote, respectively, the unit-cell volumes of diamond and silicon.

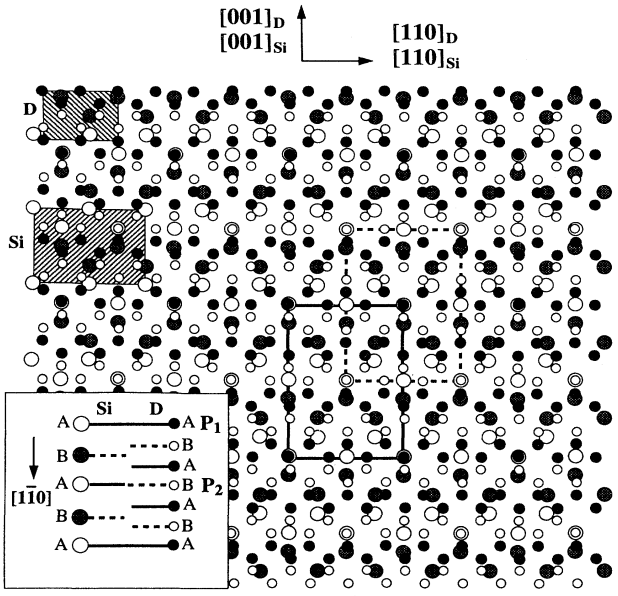

FIG. 10. [1$\bar{1}$0] projection of the $\Sigma_D 54/\Sigma_{Si} 16$ NCSL which is formed by compressively straining the silicon lattice by 1.5% along the three basic axes. Small circles stand for the carbon atoms and large ones for the silicon atoms. The different colors white, gray, and black mark the stacking sequence in the [1$\bar{1}$0] direction. The solid-line frame denotes a repeat unit of the NCSL in the paper plane, and the dashed-line frame denotes the repeat unit in the plane $a_{Si}[\frac{1}{2},\frac{\bar{1}}{2},0]$ below the paper plane. Inset: the stacking sequence of silicon (left) and diamond (right) seen along the [001] direction, i.e., bottom to top in the main figure. P_1 and P_2 refer to the planes for which the unit cell of the NCSL is given in the main figure by the thick-line and dashed-line frames, respectively.

A projection of this $\Sigma_D 54/\Sigma_{Si} 16$ NCSL along the [1$\bar{1}$0] direction is shown in Fig. 10. Shaded frames outline the projection of the unit cells of diamond and silicon. Small circles stand for the carbon atoms and large circles denote the silicon atoms. As indicated in the inset, the color, black and white in the case of diamond and white and gray in the case of silicon, indicates the two different position levels with respect to the stacking sequence of *A*, *B*, *A*, *B*... along the [1$\bar{1}$0] viewing direction. This means that, along the viewing direction, the atoms represented by the small white circles are in a plane shifted by the vector $a_D[\frac{1}{4},\frac{\bar{1}}{4},0]$ with respect to the plane of the small black circles while the large gray circles are shifted by $a_{Si}[\frac{1}{4},\frac{\bar{1}}{4},0]$ with respect to the large white circles. The large frame in the center (thick solid line) traces out the smallest repeat unit of the NCSL in the paper plane (P_1 in the inset), while the dashed-line frame shows the NCSL in the position of $a_{Si}[\frac{1}{2},\frac{\bar{1}}{2},0]$ (P_2 in the inset). We see that, in three dimensions, the 3:2 registry leads to two types of coincident atom sites. The first type concerns silicon on *A*-type planes coinciding with carbon on *A*-type planes of diamond. The second type combines Si on *A*-type planes and C on *B*-type planes. We note that the same NCSL is obtained when the diamond crystal is rotated around the [1$\bar{1}$0] axis by $\pm 70.5°$ or by $\pm 109.5°$. In all these cases, one set of {111} planes of diamond is parallel to one set of {111} planes of silicon. The rotated crystals have a twin relation with the nonrotated crystal.

Figure 11 depicts the NCSL corresponding to the orientation relation of $(1\bar{1}0)_D \| (1\bar{1}0)_{Si}$, $[116]_D \| [001]_{Si}$, and $[33\bar{1}]_D \| [110]_{Si}$, which we found experimentally in the case shown in Fig. 8. Here the silicon lattice is un-

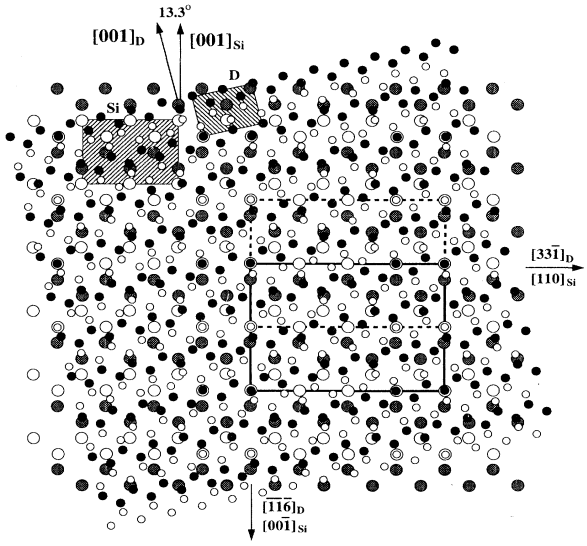

FIG. 11. The $\Sigma_D 57/\Sigma_{Si} 16$ NCSL for the interface with the misorientation angle of 13.3° around [1$\bar{1}$0]. It was constructed by straining the silicon lattice expansively in the (1$\bar{1}$0) plane by 1.22% and compressively perpendicular to this plane by 1.5%. The meaning of the symbols is the same as in Fig. 10.

changed, with respect to the ideal case of Figs. 9 and 10, while the diamond lattice is tilted around the $[1\bar{1}0]$ direction by 13.3°. This NCSL was constructed by straining the silicon lattice expansively in the $(1\bar{1}0)$ plane by 1.22% (corresponding to $\delta=-1.22\%$) and compressively perpendicular to this plane by 1.5% (corresponding to the respective value of δ discussed above). This is in contrast to the ideal case, where the introduced strain is uniform in all three dimensions. All symbols in Fig. 11 have correspondingly the same meaning as those in Fig. 10. The smallest repeat unit of the NCSL is indicated by a solid-line frame in the paper plane and a dashed-line frame for the positions $a_{\mathrm{Si}}[\frac{1}{2},\frac{\bar{1}}{2},0]$ below the paper plane. As is seen from this figure, the smallest repeat unit of the NCSL includes two coincidence atom sites. Accordingly the NCSL is characterized by the ratio $\Sigma_{\mathrm{D}}57/\Sigma_{\mathrm{Si}}16$ and $R=3.56$, i.e., a value very close to the ideal one of 3.53.

V. DISCUSSION

From our electron-microscopic observations and the crystallographic investigation of the possible interface orientation relations between the diamond film and the silicon substrate, we can conclude that the growth of the film on a clean surface of silicon follows, in many cases, specific crystallographic relations. These may be considered to be linked to the atom coincidence relations of two materials in the interfaces. Although, due to the resolution limit of the microscope, the present investigation was limited to the $\langle 110\rangle$ tilt interfaces, we can draw some more general conclusions on the modes of epitaxial growth of diamond films on silicon substrates.

The two orientation relations observed in the examples of Figs. 4 and 8 produce two of the highest density NCSL's in the classes of the $\langle 110\rangle$-, $\langle 100\rangle$-, and $\langle 111\rangle$-rotated interfaces of diamond to silicon with a mismatch of $\delta<2\%$. Although many grains were found with small-angle deviations from these exact misorientation angles for the NCSL, they are still in the corresponding class of the near-coincidence interfaces. The small misorientation is compensated for by forming interfacial dislocations which are embedded in the low-energy interfaces associated with the high density of the near-coincidence atom sites.[13] Analogous to the grain boundary dislocations discussed by Balluffi, Brokman, and King,[13] the nature of the interfacial dislocations described here is, in principle, different from that of misfit dislocations occurring in interfaces. The former originate from the angle deviation from the exact misorientation angle for a CSL, while the latter are induced by the lattice mismatch between the two crystals when they join to form an interface. The Burgers vector of misfit dislocations is related to the basic lattice, while the interfacial dislocations are described on the basis of the displacement shift complete (DSC) lattice which is spanned by those displacement vectors of lattice 2 with respect to lattice 1 which cause shifts of the complete CSL.[12,13]

From the lattice images of the interfaces of diamond to silicon, we could infer that the dislocation configuration varies with the misorientation angle. The total number of the 60° $\frac{a}{2}\langle 110\rangle$ dislocations related to the $\{111\}$-type terminating planes remains almost unchanged within a certain range of misorientation angle, which in the present work is about 15°. However, these dislocations react when they meet each other. As a result, other types of dislocations can occur in the interface. For the ideal orientation relations, i.e., the basic axes of the two materials parallel to each other, the same number of (111) and $(\bar{1}\,\bar{1}1)$ terminating planes occurs. Accordingly, the number of 60° $\frac{a}{2}[101]$ or $\frac{a}{2}[011]$ dislocations is the same as that of the 60° $\frac{a}{2}[01\bar{1}]$ or $\frac{a}{2}[10\bar{1}]$ dislocations. When the two types of dislocations react, additional dislocations are formed according to the relations

$$\frac{a}{2}[101]+\frac{a}{2}[01\bar{1}]\rightarrow\frac{a}{2}[110]\,, \tag{3a}$$

$$\frac{a}{2}[011]+\frac{a}{2}[10\bar{1}]\rightarrow\frac{a}{2}[110]\,. \tag{3b}$$

The resulting dislocations are Lomer dislocations, i.e., pure edge dislocations, whose Burgers vector lies in the interface plane. These dislocations are most efficient for the accommodation of the mismatch of the two lattices. It is obvious that both reactions are energetically favorable. Therefore the dislocation configuration at the interface consists of both 60° and Lomer dislocations. The latter are composed of two interacting 60° dislocations. This configuration was also found at the interface between GaAs and Si.[14] In the extreme situation, the dislocation configuration at the interfaces exhibiting the ideal orientation relation should be a network of Lomer dislocations. This can minimize the energy of the interface by reducing the number of dislocations existing at the interface.

For cases where the diamond grains are tilted or rotated away from the ideal orientation, e.g., tilted around the $[1\bar{1}0]$ axis as shown in Figs. 3, 6, and 8, it is impossible to completely eliminate the 60° dislocations by the above reaction since the two types of dislocation do not occur in equal numbers. The total Burgers vector of the remaining 60° dislocations includes a component perpendicular to the interface plane which is required to compensate for the misorientation of the grains. In fact, the number of the $\frac{a}{2}\langle 110\rangle$ dislocations at these interfaces should be larger than that in the ideal case. As a consequence the total energy associated with dislocations is higher, thus favoring interfaces with close to ideal orientations.

Finally we note that the stability of the interface is not only determined by the density of the atomic coincidence sites and the dislocation configuration at the interface, but also by the electronic structure of the interface. Therefore, in order to arrive at a more complete understanding of the interfacial structure, the electronic contribution to the interfacial energy has to be considered and total-energy calculations of the different types of interfaces are required.[15]

ACKNOWLEDGMENTS

The authors would like to thank Dr. C.-P. Klages and Dr. W. Jäger for stimulating discussions.

[1]X. Jiang and C.-P. Klages, Diamond Relat. Mater. **2**, 1112 (1993).
[2]X. Jiang, C.-P. Klages, R. Zachai, M. Hartweg, and H.-J. Füsser, Appl. Phys. Lett. **62**, 3438 (1993).
[3]X. Jiang, K. Schiffmann, and C.-P. Klages, Phys. Rev. B **50**, 8402 (1994).
[4]B. E. Williams and J. T. Glass, J. Mater. Res. **4**, 373 (1989).
[5]B. R. Stoner, G.-H. Ma, S. D. Wolter, and J. T. Glass, Phys. Rev. B **45**, 11 067 (1992).
[6]N. Jiang, Z. Zhang, B. W. Sun, and D. Shi, Appl. Phys. Lett. **63**, 328 (1993).
[7]Y. Tzou, J. Bruley, F. Ernst, M. Rühle, and R. Raj, J. Mater. Res. **9**, 1566 (1994).
[8]R. E. Clausing, L. Heatherly, L. L. Horton, E. D. Specht, G. M. Begun, and Z. L. Wang, Diamond Relat. Mater. **1**, 411 (1992).
[9]C. Wild, R. Kohl, N. Herres, W. Müller-Sebert, and P. Koidl, Diamond Relat. Mater. **3**, 373 (1994).
[10]X. Jiang, C.-P. Klages, R. Zachai, M. Hartweg, and H.-J. Füsser, Diamond Relat. Mater. **2**, 407 (1993).
[11]D. Shechtman, A. Feldman, M. D. Vaudin, and J. Hutchison, Appl. Phys. Lett. **62**, 487 (1993).
[12]W. Bollmann, *Crystal Defects and Crystalline Interfaces* (Springer-Verlag, Berlin, 1970).
[13]R. W. Balluffi, A. Brokman, and A. H. King, Data Metall. **30**, 1453 (1982).
[14]D. Gerthsen, Philos. Mag. A **67**, 1365 (1993).
[15]W. S. Verwoerd, K. Osuch, and P. Badziag, Surf. Sci. **312**, 221 (1994).

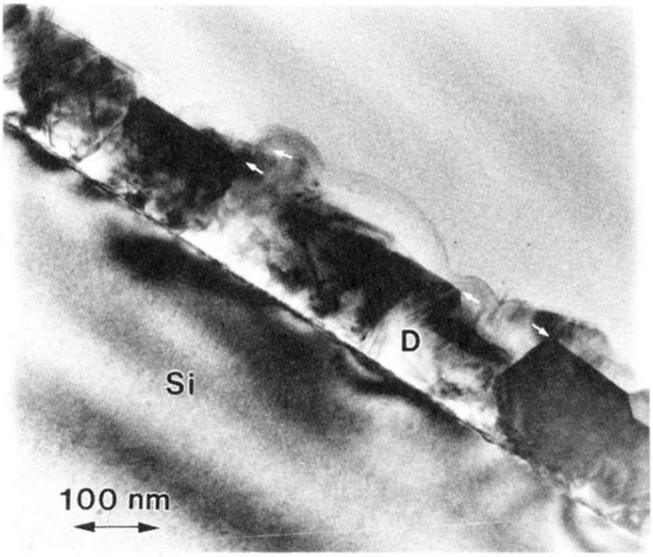

FIG. 1. A low-magnification overview of a highly (001)-oriented diamond film (D) on a (001) silicon substrate (Si). The viewing direction is parallel to the $[1\bar{1}0]$ zone axis of silicon. The well-oriented grains of diamond exhibit a polygonal morphology. Small arrows indicate the projected (001) plane of the diamond grains.

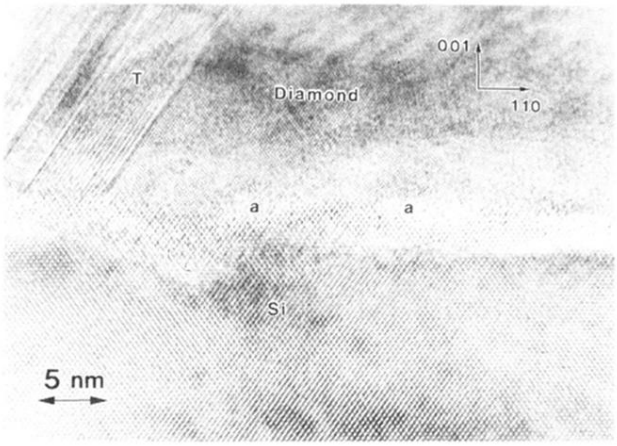

FIG. 2. A [$1\bar{1}0$] lattice-fringe picture of the interface between a diamond grain and the silicon substrate. The diamond grain is oriented with its basic axes parallel to those of the silicon substrate (ideal orientation). Two small amorphous zones in the interface are marked by *a*. Twin lamellae (*T*) are visible on the left-hand side of the diamond grain.

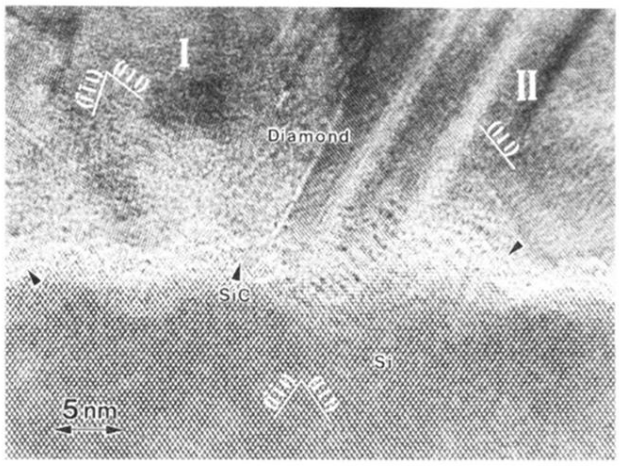

FIG. 3. Interface of two diamond grains to the silicon substrate. The two grains deviate from the ideal orientation by a rotation around the $[1\bar{1}0]$ axis (grain I) and the [111] axis (grain II). Small β-SiC particles are denoted by arrowheads. The basic axes of these precipitates are parallel to those of silicon.

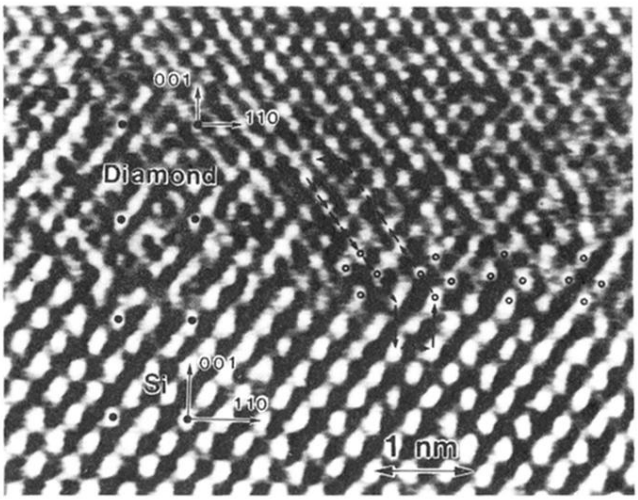

FIG. 4. A $[1\bar{1}0]$ lattice-fringe image of the interface between diamond and silicon. The diamond grain has a perfectly epitaxial orientation. The small circles allow the continuity of the two lattices across the interface to be verified. A Burgers circuit composed of small arrows demonstrates the Burgers vector of the dislocations which are related to the terminating $\{111\}$-type planes at the interface. The black dots indicate a $\Sigma_D 54/\Sigma_{Si}$ 16 near-coincidence-site lattice (NCSL).

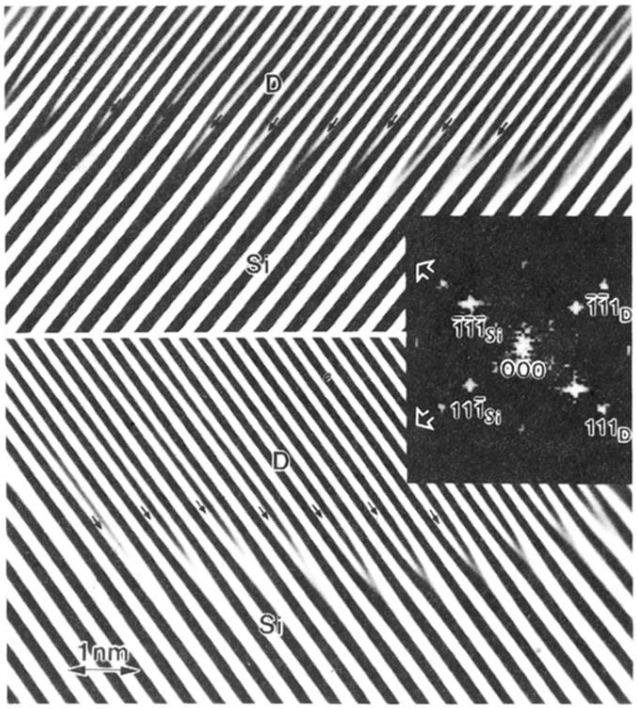

FIG. 5. Lattice-fringe pattern obtained by Fourier filtering the image of the Fig. 4. In the image synthesis the (111)-spot row (upper picture) and the $(\bar{1}\,\bar{1}1)$-spot row (lower picture) of the corresponding power spectrum were used, which is shown as an inset. Small arrows mark the terminating planes at the interface.

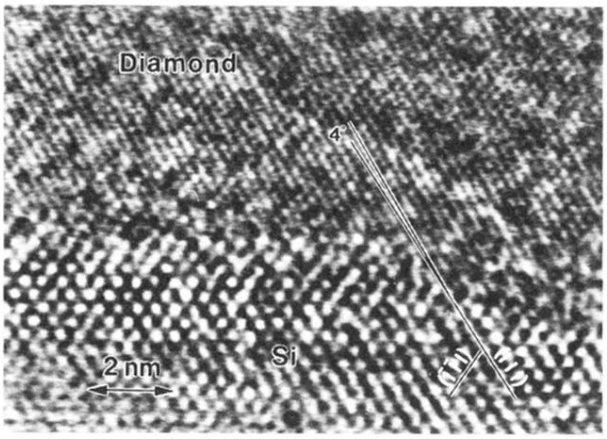

FIG. 6. A [1$\bar{1}$0] lattice-fringe image showing a diamond grain which exhibits a 4° deviation from the ideal orientation. Such small-angle deviations are compensated for by unequal numbers of the ($\bar{1}\,\bar{1}$1) and (111) terminating planes.

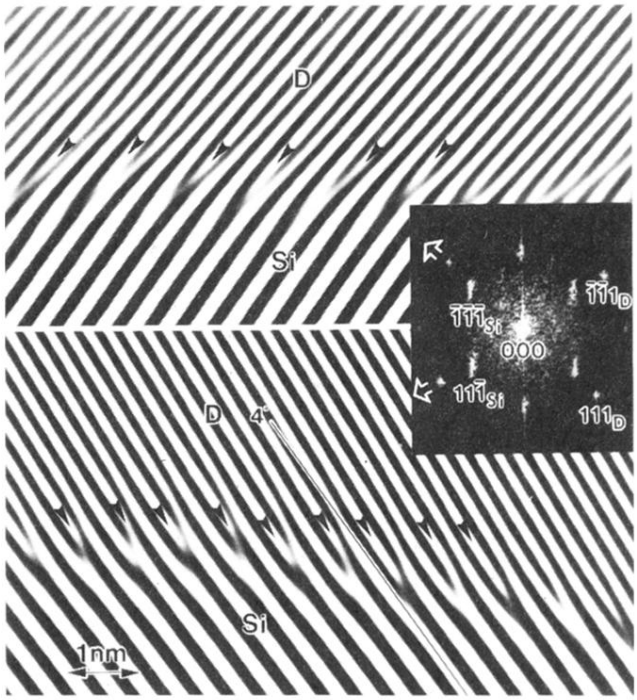

FIG. 7. Fourier-filtered images obtained from Fig. 6 by using the (111)-spot row (upper picture) and the ($\bar{1}\,\bar{1}1$)-spot row (lower picture) of the corresponding power spectrum shown as an inset. They show a different configuration of the terminating planes (marked by arrowheads) in comparison with the ideal situation (Fig. 5).

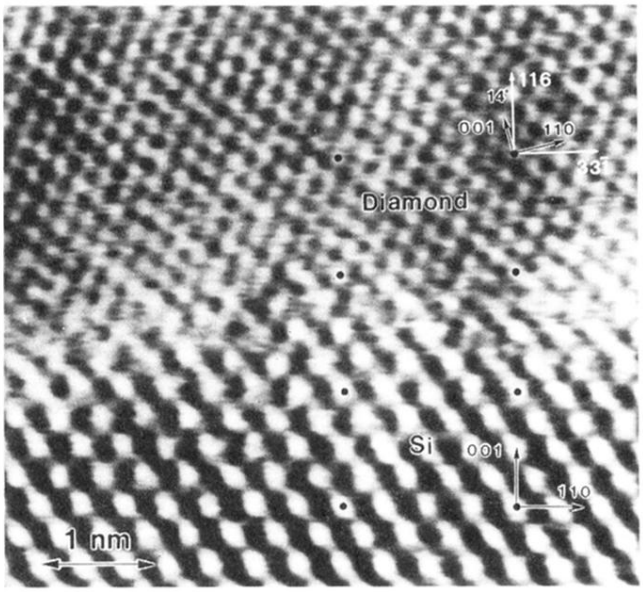

FIG. 8. The interface between a diamond grain and the silicon substrate. This grain is rotated by 14° around the $[1\bar{1}0]$ axis with respect to the silicon substrate. For this misorientation angle, a $\Sigma_D 57/\Sigma_{Si} 16$ NCSL is formed. The periodicity of the NCSL is marked by black dots.